IEEE Access
Multidisciplinary ⋮ Rapid Review ⋮ Open Access Journal

Received 21 September 2023, accepted 11 October 2023, date of publication 18 October 2023, date of current version 25 October 2023.

Digital Object Identifier 10.1109/ACCESS.2023.3325678

RESEARCH ARTICLE

RIS-Aided mmWave Network Planning Toward Connectivity Enhancement and Minimal Electromagnetic Field Exposure

BO YIN, WOUT JOSEPH, (Senior Member, IEEE), AND MARGOT DERUYCK, (Member, IEEE)
Department of Information Technology, IMEC, Ghent University, 9052 Ghent, Belgium

Corresponding author: Bo Yin (bo.yin@ugent.be)

The work of Bo Yin was supported by the China Scholarship Council under Grant 202206150004. The work of Margot Deruyck was supported by the Research Foundation Flanders (FWO-V) under Grant 12Z5621N.

ABSTRACT The utilization of millimeter wave (mmWave) technology has emerged as a key enabler for the advancement of future wireless networks. However, the widespread deployment of mmWave communication is impeded by the challenges posed by its harsh propagation characteristics. To overcome this limitation, the reconfigurable intelligent surface (RIS) is envisioned as a potential solution to enhance mmWave coverage by intelligently controlling signal reflections. In this paper, we study a RIS-aided multi-user downlink multiple-input single-output (MISO) mmWave network. We formulate the RIS-aided network planning as mixed-integer nonlinear programming (MINLP) by jointly optimizing the placement of infrastructure and link associations to maximize the connectivity while considering electromagnetic field (EMF) exposure constraints. To address this intractable problem, we transform it into mixed-integer linear programming (MILP) and then propose a power-efficient algorithm to solve it effectively. Numerical results show that substantial performance improvements are achieved by incorporating the RIS in mmWave networks. In particular, the proposed algorithm outperforms the conventional benchmark that does not employ the RIS, with up to 20% enhancement in connectivity and 14% reduction in EMF exposure.

INDEX TERMS Millimeter wave (mmWave), connectivity maximization, electromagnetic field (EMF) exposure, reconfigurable intelligent surface (RIS), network planning.

I. INTRODUCTION

The fifth-generation (5G) and beyond 5G (B5G) wireless networks have been extensively envisioned to realize ubiquitous connectivity, addressing the essential performance requirements of enhanced mobile broadband (eMBB), ultra-reliable and low-latency communications (URLLC), and massive machine-type communications (mMTC) [1]. Moreover, the dramatically growing number of connected devices and increasing demand for high-capacity data transmission have driven the need for advanced wireless communication technologies. For example, with an estimated count of 29 billion connected devices projected by 2023 [2], the demand for spectrum allocation is expected to grow exponentially, which calls for innovative approaches and solutions to efficiently manage and allocate spectrum resources, ensuring reliable and high-quality connectivity.

Recently, two promising technologies, namely millimeter-wave (mmWave) and reconfigurable intelligent surface (RIS), also known as intelligent reflecting surface (IRS), have emerged as potential solutions for enhancing communication capacity and enabling massive connectivity in 5G and B5G wireless networks. The mmWave communication operates in the frequency range of 30 to 300 GHz,[1] providing access to extremely large bandwidths and enabling significantly higher data rates and capacity compared to traditional sub-6 GHz band wireless networks [3], [4], [5], [6], [7].

The associate editor coordinating the review of this manuscript and approving it for publication was Kashif Sharif.

[1]While the mmWave spectrum is typically defined as the frequency range between 30 and 300 GHz, it is the band specifically ranging from 24 up to 100 GHz that is expected to be utilized for 5G and B5G communications.

© 2023 The Authors. This work is licensed under a Creative Commons Attribution-NonCommercial-NoDerivatives 4.0 License.
For more information, see https://creativecommons.org/licenses/by-nc-nd/4.0/

On the other hand, due to the harsh propagation characteristics of mmWave, such as scattering, diffraction, and penetration loss [3], [4], mmWave signals face challenges related to coverage limitations and susceptibility to blockages. For instance, the impact of blockage effects on both line-of-sight (LOS) paths and non-line-of-sight (NLOS) paths is particularly pronounced [3]. As a result, the blockage effect leads to substantial differences in the path loss characteristics between LOS and NLOS scenarios, posing significant challenges for reliable communication in mmWave networks.

To overcome the limitations of mmWave communication, RIS has emerged as a potential solution. RIS consists of a number of passive elements that can reflect and manipulate signals, enhancing the coverage of mmWave communication in 5G and B5G wireless networks [8], [9], [10], [11]. By strategically controlling the phase shifts of RIS elements, reflected signals can be focused towards the desired direction, mitigating the effects of blockages and enhancing the overall coverage and capacity of mmWave communication. For example, RIS is typically exploited to enhance the mmWave signals coverage when the direct links between the base station (BS) and user equipment (UE) are unavailable. Additionally, RIS offers the advantages of low cost and low power consumption for optimizing wireless networks due to its passive structure. Therefore, the integration of RIS with mmWave communication has the potential to revolutionize wireless networks, improving coverage, capacity, and reliability.

Although the integration of RIS in mmWave networks brings forth numerous benefits, it is crucial to account for electromagnetic field (EMF) exposure [12], [13], [14]. Guidelines for non-ionizing radio frequency radiations have been published by the International Commission on Non-Ionizing Radiation Protection (ICNIRP) [15]. Public concerns regarding EMF radiation have increased, particularly in the context of mmWave networks [16], [17], [18], [19]. Hence, it becomes imperative to develop network planning strategies that not only optimize connectivity and system performance but also adhere to strict EMF exposure limits. Striking a balance between connectivity enhancement and human exposure is a critical aspect of the design and deployment of RIS-aided mmWave networks.

A. RELATED WORKS

RIS-aided mmWave networks for coverage enhancement have already been investigated [11], [20], [21], [22], [23], [24]. Li et al. [11] study the coverage probability of the RIS-aided outdoor-to-indoor mmWave networks and derive a closed-form approximation for the coverage probability, which provides insights into the performance of RIS-aided network deployment. Albanese et al. [20] present a framework for joint multi-RIS deployment and UE association in a multi-user mmWave network, aiming to improve the network coverage. To tackle the challenges posed by large-scale scenarios, a RIS-aided network planning algorithm is proposed to provide an iterative solution to the max-min throughput optimization problem. The authors of [21] create a smart radio connection where RISs are installed at candidate sites to improve communication between BSs and test points, further formulate the coverage planning problem with the objective of maximizing the sum-throughput, and solve it using well-established planning methods. In [22], the weighted sum-rate problem with joint active and passive beamforming is maximized by using an alternating iterative algorithm with decoupling the active and passive beamforming variables. Nemati et al. [23] analyze the coverage of a RIS-assisted large-scale mmWave cellular network using stochastic geometry and derive closed-form expressions for the peak reflection power of a RIS and the downlink signal-to-interference ratio coverage. The authors of [24] minimize the system sum rate by jointly optimizing the precoding strategy of the BS and RIS parameters for addressing massive IoT access challenges in mmWave networks. On the other hand, in [17], authors consider the optimization problem of maximizing the energy efficiency in a RIS-aided communication system, taking into account both maximum power constraints and maximum EMF exposure constraints. Ibraiwish et al. [18] propose an EMF-aware scheme for RIS-aided networks, which aims at minimizing the EMF exposure subject to quality-of-service (QoS) constraints. The authors of [19] consider a RIS-assisted system with joint optimization of the beamforming vectors, power allocation, and the phase shifts at the RIS elements, and propose a projected gradient descent-based optimization strategy to maximize the minimum signal-to-interference-plus-noise ratio (SINR) subject to constraints on the power consumed by the users.

Predictably, RISs play a crucial role in enhancing the connectivity and reducing the EMF exposure of the mmWave networks. Unfortunately, the works presented in [11], [16], [17], [18], [19], [20], [21], [22], [23], and [24] focus on only one of the aspects, which is not sufficient to tackle the issue in this context. This motivates our work.

B. MAIN CONTRIBUTIONS

In this paper, different from the above-mentioned works, we aim at exploring a RIS-aided general network planning framework by focusing on maximizing connectivity as the primary optimization objective of the system while taking into account the EMF exposure constraints. Additionally, we also study the objective of minimizing EMF exposure under a given coverage rate. Specifically, we consider a RIS-aided multi-user downlink multiple-input single-output (MISO) mmWave network, in which both BSs and RISs are strategically deployed at specific sites, facilitating communication with UEs. In our proposed model, each UE can communicate with the BS through different links for the purpose of connectivity enhancement. Our study emphasizes the importance of achieving high connectivity while ensuring compliance with EMF exposure limit, providing a unique perspective in the context of RIS-aided mmWave networks. The main contributions of this paper are summarized as follows:

TABLE 1. List of key symbols.

Symbol	Description
K, L	Number of RISs and BSs
N	Number of reflection elements at the RIS
M	Number of antennas at the BS
$\mathcal{T}$	Set of all UEs
B	Bandwidth
E	Downlink global EMF exposure
$E_{\max}$	Maximum electric field strength in $\mathcal{R}$
σ_t^2	Noise variance at the t-th UE
$G_{l,k}$	Channel from the l-th BS to the k-th RIS
$h_{l,t}$	Channel from the l-th BS to the t-th UE
$g_{k,t}$	Channel from the k-th RIS to the t-th UE
$\theta_{k,i}$	Phase coefficient of the i-th element at the k-th RIS
$\alpha_{l,t}$	Indicator to check if the l-th BS serves the t-th UE by BS-UE channel
$\beta_{l,k,t}$	Indicator to check if the l-th BS serves the t-th UE by BS-RIS-UE channel
$\gamma_{l,k,t}$	Indicator to check if the l-th BS serves the$t$-th UE by COM-BS-RIS channel
$w_{l,t}$	Beamforming vector of the l-th BS for the t-th UE
ϖ	Weighting coefficient related to exposure
x_l, y_k	Indicator to check if the l-th BS and the k-th RIS are installed
$\zeta^B, \zeta^R, \zeta^{\text{tot}}$	Cost of installing the BS, RIS, and total cost
$P_{\max}$	Maximum transmit power of the BS
$E_{\lim}$	Limit EMF exposure
$R_t^{\min}$	Required minimum QoS requirement of the t-th UE
CR	Required coverage rate

- We investigate a RIS-aided multi-user downlink MISO mmWave network architecture that provides flexible communication links between BSs and UEs, allowing for enhanced connectivity and improved system performance. We specifically consider the impact of maximum transmit power constraints and additional EMF exposure constraints, which are crucial factors in the context of massive 5G and B5G connectivity.
- We formulate the RIS-aided network planning optimization problem as two distinct mixed-integer nonlinear programming (MINLP) problems, depending on the specific objectives and constraints of the system. To facilitate efficient solution methods, we transform them into mixed-integer linear programming (MILP) problems and then propose the RIS-aided power-efficient (RISP) algorithm to effectively address these MILP problems.
- The comprehensive numerical results highlight the significant performance improvements achieved by the RIS-aided mmWave networks optimized by using the RISP algorithm. The system demonstrates enhanced connectivity and reduced EMF exposure compared to traditional networks. These findings underscore the effectiveness of incorporating RIS with mmWave networks and utilizing the RISP to optimize system performance.

C. ORGANIZATION AND NOTATIONS

The remainder of this paper is organized as follows. Section II outlines the system, channel, and exposure models.

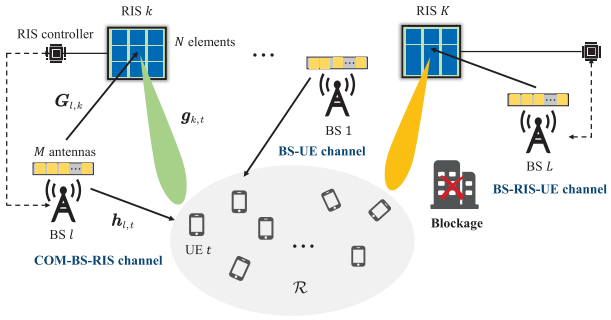

FIGURE 1. RIS-aided downlink multi-user mmWave networks.

In Section III, we formulate the joint optimization problems, considering the specific objectives and constraints of the system. Then, in Section IV, a RIS-aided network planning algorithm is proposed to solve the formulated optimization problems. Simulation results are presented in Section V to evaluate the effectiveness of the proposed algorithm, and Section VI concludes this paper.

Notations: We use calligraphy letters to represent sets. Matrices and vectors are in the form of upper-case and lower-case bold letters, respectively. $(\cdot)^*$, $(\cdot)^T$ and $(\cdot)^H$ stand for vector or matrix conjugate, transposition and Hermitian transposition, respectively. We use $\mathcal{CN}(\cdot,\cdot)$ to denote the complex Gaussian distribution, and $\mathbb{E}(\cdot)$ to denote expectation. The N-dimensional real and complex spaces are denoted by $\mathbb{R}^N$ and $\mathbb{C}^N$, respectively. The L2-norm of a vector is denoted by $\|\cdot\|$. In addition, the key symbols involved in the paper are also listed and explained in Table 1.

II. SYSTEM MODEL

A. RIS-AIDED DOWNLINK MMWAVE NETWORKS

In this paper, we consider a RIS-aided multi-user downlink MISO[2] mmWave (operating at 28 GHz [25]) network, as depicted in Figure 1, where K RISs each equipped with a uniform planar array (UPA) of N reflecting elements are deployed to assist L BSs each equipped with a uniform linear array (ULA) consisting of M antennas to enhance the wireless communication within a given area of $\mathcal{R}$. The single-antenna UEs acquiring data from the BS are assumed to be randomly distributed in $\mathcal{R}$, and we denote the collection of all UEs as $\mathcal{T}$. The BS can establish communication with the UE via three distinct links:

- The direct link between the BS and UE, i.e., BS-UE channel.
- The reflected link through the RIS, i.e., BS-RIS-UE channel.
- The combined link of the BS-UE and BS-RIS-UE channels, i.e., COM-BS-RIS channel.

[2]Since our objectives focus on the network side and try to obtain the theoretical bound on the connectivity and exposure, and our proposed algorithm can also be extended to the case of MIMO scenario, for simplicity and analysis, we investigate the exposure and connectivity in the downlink, i.e., MISO system, in this work.

Each RIS is controlled by a smart RIS controller with the capability to adjust the phases and amplitudes of the reflecting elements independently, thereby reflecting the incident signals to the desired direction.

The flat-fading channel model is considered for all channels, in which channel coefficients remain constant within one transmission time interval (TTI). Let $\boldsymbol{G}_{l,k} \in \mathbb{C}^{N\times M}$, $\boldsymbol{h}_{l,t} \in \mathbb{C}^{M\times 1}$, and $\boldsymbol{g}_{k,t} \in \mathbb{C}^{N\times 1}$ denote the equivalent baseband channel coefficients from the l-th BS to the k-th RIS, the l-th BS to the t-th UE, and the k-th RIS to the t-th UE, respectively. Let $\boldsymbol{\theta}_k = \left[e^{j\theta_{k,1}}, \ldots, e^{j\theta_{k,N}}\right] \in \mathbb{C}^{N\times 1}$ and define a diagonal matrix $\boldsymbol{\Theta}_k = \mathrm{diag}\left(\boldsymbol{\theta}_k\right) \in \mathbb{C}^{N\times N}$ as the adjustable reflection coefficients at the k-th RIS, where $\theta_{k,i} \in [0, 2\pi)$ denotes the phase shift coefficient of the i-th passive element of the k-th RIS.

We define a binary variable $\alpha_{l,t}$ to identify the association between the BS and UE, i.e., $\alpha_{l,t} = 1$ if the t-th UE is connected to the l-th BS via the BS-UE channel and $\alpha_{l,t} = 0$ otherwise. Similarly, a introduced binary variable $\beta_{l,k,t}$ indicates the association between the BS, RIS, and UE, i.e., $\beta_{l,k,t} = 1$ if the t-th UE is connected to the l-th BS with the assistance of the k-th RIS through the BS-RIS-UE channel, and $\beta_{l,k,t} = 0$ otherwise.

Remark 1: With the introduction of $\alpha_{l,t}$ and $\beta_{l,k,t}$, there are five possible ways for the t-th UE to communicate with the BS: 1) only $\alpha_{l,t} = 1$, namely BS-UE channel; 2) only $\beta_{l,k,t} = 1$, namely BS-RIS-UE channel; 3) $\alpha_{l,t} = 1$ and $\beta_{l,k,t} = 1$ with identical l, namely COM-BS-RIS channel; 4) $\alpha_{l,t} = 1$ and $\beta_{l,k,t} = 1$ with different l; and 5) $\alpha_{l,t} = 0$ and $\beta_{l,k,t} = 0$, namely the t-th UE can not be connected.

Assume that $s_t \in \mathbb{C}$ is the transmitted signal from the BS for the t-th UE with normalized power, i.e., $\mathbb{E}(|s_t|^2) = 1$. We consider linear transmit precoding at the BS with a dedicated beamforming vector assigned to each UE. Denote $\boldsymbol{w}_{l,t} \in \mathbb{C}^{M\times 1}$ as the beamforming vector of the l-th BS for the t-th UE. Then, the received signal $y_t \in \mathbb{C}$ at the t-th UE can be expressed as

$$y_t = \sum_{l,k}\left(\beta_{l,k,t}\boldsymbol{g}_{k,t}^H\boldsymbol{\Theta}_k\boldsymbol{G}_{l,k} + \alpha_{l,t}\boldsymbol{h}_{l,t}^H\right)\sum_{t\in\mathcal{T}}\boldsymbol{w}_{l,t}s_t + n_t, \quad (1)$$

where $n_t \sim \mathcal{CN}\left(0, \sigma_t^2\right)$ represents the additive white Gaussian noise (AWGN) at the receiver of the t-th UE. Therefore, the received instantaneous SINR $\eta_t \in \mathbb{R}$ of the t-th UE is given by

$$\eta_t = \frac{\left|\sum_{l,k}\left(\beta_{l,k,t}\boldsymbol{g}_{k,t}^H\boldsymbol{\Theta}_k\boldsymbol{G}_{l,k} + \alpha_{l,t}\boldsymbol{h}_{l,t}^H\right)\boldsymbol{w}_{l,t}\right|^2}{\sum_{j\neq t}\left|\sum_{l,k}\left(\beta_{l,k,j}\boldsymbol{g}_{k,t}^H\boldsymbol{\Theta}_k\boldsymbol{G}_{l,k} + \alpha_{l,j}\boldsymbol{h}_{l,t}^H\right)\boldsymbol{w}_{l,j}\right|^2 + \sigma_t^2}. \quad (2)$$

Accordingly, the achievable data rate $r_t \in \mathbb{R}$ of the t-th UE can be computed by

$$r_t = B\log_2\left(1+\eta_t\right), \quad \forall t \in \mathcal{T}, \quad (3)$$

where B is the bandwidth.

B. MMWAVE CHANNEL MODEL

According to the geographic Saleh-Valenzuela channel model typically used for mmWave communication [5], [6], [26], the channel coefficients $\boldsymbol{h}_{l,t}, \boldsymbol{g}_{k,t}$, and $\boldsymbol{G}_{l,k}$ can be further modeled as

$$\boldsymbol{h}_{l,t} = \sqrt{\frac{M}{U_{l,t}}}\sum_{\ell}^{U_{l,t}}\kappa_{l,t}^{(\ell)}\boldsymbol{a}_M\left(\phi_{l,t}^{(\ell)}, \hat{\phi}_{l,t}^{(\ell)}\right), \quad (4)$$

$$\boldsymbol{g}_{k,t} = \sqrt{\frac{N}{Q_{k,t}}}\sum_{\ell}^{Q_{k,t}}\iota_{k,t}^{(\ell)}\boldsymbol{a}_N\left(\varphi_{k,t}^{(\ell)}, \hat{\varphi}_{k,t}^{(\ell)}\right), \text{ and,} \quad (5)$$

$$\boldsymbol{G}_{l,k} = \sqrt{\frac{MN}{F_{l,k}}}\sum_{\ell}^{F_{l,k}}\rho_{l,k}^{(\ell)}\boldsymbol{a}_N\left(\psi_{l,k}^{(\ell)}, \hat{\psi}_{l,k}^{(\ell)}\right)\boldsymbol{a}_M^H\left(\omega_{l,k}^{(\ell)}, \hat{\omega}_{l,k}^{(\ell)}\right), \quad (6)$$

respectively, where $U_{l,t}$, $Q_{k,t}$, and $F_{l,k}$ denote the total number of propagation paths including the LOS and NLOS components ($\ell = 0$ represents the LOS path) between the l-th BS and the t-th UE, between the k-th RIS and the t-th UE, and between the l-th BS and the k-th RIS, respectively. The corresponding complex gains of the ℓ-th path are represented by $\kappa_{l,t}^{(\ell)}$, $\iota_{k,t}^{(\ell)}$, and $\rho_{l,k}^{(\ell)}$ respectively. The azimuth (elevation) angles of arrival (AoAs) and departure (AoDs) of the ℓ-th path between the l-th BS and the k-th RIS are denoted as $\psi_{l,k}^{(\ell)}$ ($\hat{\psi}_{l,k}^{(\ell)}$) and $\omega_{l,k}^{(\ell)}$ ($\hat{\omega}_{l,k}^{(\ell)}$), respectively. Similarly, $\phi_{l,t}^{(\ell)}$ ($\hat{\phi}_{l,t}^{(\ell)}$) and $\varphi_{k,t}^{(\ell)}$ ($\hat{\varphi}_{k,t}^{(\ell)}$) are the azimuth (elevation) AoDs of the ℓ-th path between the l-th BS and the t-th UE and between the k-th RIS and the t-th UE, respectively. The $\boldsymbol{a}_M(x_a, x_e) \in \mathbb{C}^{M\times 1}$ and $\boldsymbol{a}_N(\hat{x}_a, \hat{x}_e) \in \mathbb{C}^{N\times 1}$ represent the normalized array response vectors at an azimuth (elevation) angle of x_a (x_e) and $\hat{x}_a$ ($\hat{x}_e$), respectively, where, for example, $x_a = \phi_{l,t}^{(\ell)}$ and $x_e = \hat{\phi}_{l,t}^{(\ell)}$.

Note that the response vectors $\boldsymbol{a}_M(x_a, x_e)$ and $\boldsymbol{a}_N(\hat{x}_a, \hat{x}_e)$ depend only on the antenna array structure of the transmitter and receiver, and are independent of the properties of antenna elements [6]. In this paper, for an M-antenna ULA structure of the BS, the array response vector can be written as

$$\boldsymbol{a}_M(x_a) = \frac{1}{\sqrt{M}}\left[1, \ldots, e^{j(M-1)\frac{2\pi}{\lambda_c}d\sin(x_a)}\right]^T, \quad (7)$$

where λ_c is the carrier wavelength and d denotes the inter-element spacing. Due to the response of ULA array is invariant in the elevation domain, we here ignore x_e in the arguments of $\boldsymbol{a}_M$. In the case of a UPA structure with N elements of the RIS, the array response vector can be written as

$$\boldsymbol{a}_N(\hat{x}_a, \hat{x}_e) = \frac{1}{\sqrt{N}}\Bigg[1, \ldots, e^{j\frac{2\pi}{\lambda_c}d\left(m\sin(\hat{x}_a)\sin(\hat{x}_e)+n\cos(\hat{x}_e)\right)}, \ldots, e^{j\frac{2\pi}{\lambda_c}d\left((W-1)\sin(\hat{x}_a)\sin(\hat{x}_e)+(H-1)\cos(\hat{x}_e)\right)}\Bigg]^T, \quad (8)$$

where $0 \le m \le W-1$ and $0 \le n \le H-1$ are the horizontal and vertical indices of elements respectively and thus, the element array size of the RIS is $N = WH$.

Considering the harsh propagation characteristics of mmWave communication and power-limited high-order reflections of the RIS, the transmit power of 2 or more reflections can be ignored. As such, we here only consider LOS path for the RIS-aided propagation [9], [10], [22]. Given this assumption, (5) and (6) can be further reduced to

$$\boldsymbol{g}_{k,t} = \sqrt{N}\iota_{k,t}^{(0)}\boldsymbol{a}_N\left(\varphi_{k,t}^{(0)}, \hat{\varphi}_{k,t}^{(0)}\right), \tag{9}$$

and

$$\boldsymbol{G}_{l,k} = \sqrt{MN}\rho_{l,k}^{(0)}\boldsymbol{a}_N\left(\psi_{l,k}^{(0)}, \hat{\psi}_{l,k}^{(0)}\right)\boldsymbol{a}_M^H\left(\omega_{l,k}^{(0)}, \hat{\omega}_{l,k}^{(0)}\right), \tag{10}$$

respectively. To obtain the theoretical upper bound performance gains brought by the RIS, we assume, in this paper, the channel state information (CSI) is perfectly known at the BS as well as the issues such as beam misalignment and divergence are well addressed. The channel estimation and beam alignment for the RIS-aided mmWave systems is a complex issue which can be found in [26], [27], [28], [29], and [30].

C. EMF EXPOSURE MODEL

We define the downlink global EMF exposure, E (in V/m), as the weighted values of the average value E_{ave} (in V/m) and the maximum value $E_{\max}$ (in V/m) of the electric field strength in the region of $\mathcal{R}$ [31], i.e.,

$$E = \varpi E_{\text{ave}} + (1-\varpi)E_{\max}, \tag{11}$$

where $\varpi \in [0,\ 1]$ is the weighting coefficient related to E_{ave}, which can be chosen of equal importance, i.e., $\varpi = 0.5$ [31]. To determine the values of E_{ave} and $E_{\max}$, we estimate the downlink electric field strength at each grid (the distance between any two adjacent grids in both horizontal and vertical directions is a same constant which can be predefined). For each grid i, the electric field strength induced by the l-th BS can be modeled as [31]

$$E_{l,i} = 10^{\left(\text{EIRP}_l - 43.15 + 20\log_{10}(f_c) - \text{PL}_{l,i}\right)/20}, \tag{12}$$

where f_c is the frequency in MHz, $\text{PL}_{l,i}$ is the experienced path loss from the l-th BS to the i-th grid in dB, and EIRP_l is the theoretical maximum radiated power at the l-th BS in dBm. Note that (12) is an empirical equation based on extensive measurement campaigns, identifying the relationship between the electric field strength and path loss. Therefore, the total electric field strength caused by all contributing BS at the i-th grid E_i^{tot} can then be determined as

$$E_i^{\text{tot}} = \sqrt{\sum_{l=1}^{L} E_{l,i}^2}. \tag{13}$$

Eventually, these electric field strength values are considered for the EMF exposure evaluation.

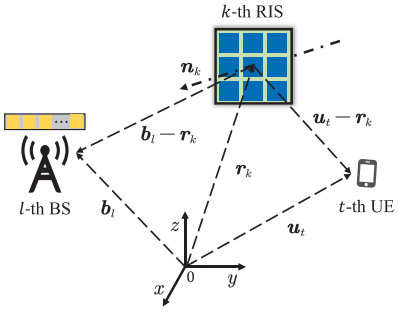

FIGURE 2. Geometric representation of the l-th BS, k-th RIS and t-th UE.

III. PROBLEM FORMULATION

To characterize the geometric representation of the system, we use $\boldsymbol{b}_l \in \mathbb{R}^{3\times 1}$, $\boldsymbol{r}_k \in \mathbb{R}^{3\times 1}$, and $\boldsymbol{u}_t \in \mathbb{R}^{3\times 1}$ to denote the location of the l-th BS, the k-th RIS center, and the t-th UE respectively in a absolute coordinate system depicted in Figure 2. Let $\boldsymbol{n}_k \in \mathbb{R}^{3\times 1}$ represent the orientation vector (normal vector) pointing to the reflecting surface of the k-th RIS. Accordingly, $\boldsymbol{b}_l - \boldsymbol{r}_k$ and $\boldsymbol{u}_t - \boldsymbol{r}_k$ represent the direction vector from the k-th RIS to the l-th BS and that to the t-th UE, respectively.

A. MAIN CONSTRAINTS

There are some main constraints to be considered while implementing the RIS for mmWave networks.

1) CONSTRAINTS FOR EACH UE

To guarantee that each UE can be served by at most one BS and one RIS, we introduce a auxiliary binary variable $\gamma_{l,k,t}$ to denote that the UE acquires data from the BS through COM-BS-RIS channel,[3] thus we have,

$$\sum_{l}\alpha_{l,t} \le 1,\ \sum_{l,k}\beta_{l,k,t} \le 1,\ \sum_{l,k}\gamma_{l,k,t} \le 1,\quad \forall t \in \mathcal{T}. \tag{14}$$

More importantly, each UE can choose up to one of the BS-UE channel, BS-RIS-UE channel and COM-BS-RIS channel to receive data from the BS, i.e.,

$$\begin{cases} \sum_{l}\alpha_{l,t} + \sum_{l,k}\beta_{l,k,t} \le 1, & \forall t \in \mathcal{T}, \\ \sum_{l}\alpha_{l,t} + \sum_{l,k}\gamma_{l,k,t} \le 1, & \forall t \in \mathcal{T}, \\ \sum_{l,k}\beta_{l,k,t} + \sum_{l,k}\gamma_{l,k,t} \le 1, & \forall t \in \mathcal{T}. \end{cases} \tag{15}$$

[3] According to **Remark 1**, for a given UE $t \in \mathcal{T}$, $\alpha_{l,t} = 1$ and $\beta_{l,k,t} = 1$ are not adequate to guarantee that l is identical, i.e., the t-th UE communicates with the l-th BS via COM-BS-RIS channel. To address this, a binary variable $\gamma_{l,k,t}$ is introduced to indicate this complex scenario for simplicity.

2) CONSTRAINTS FOR EACH BS AND RIS

We assume that the BSs and RISs can be only deployed at specific locations,[4] i.e., candidate sites (CSs). However, to indicate whether the BSs and RISs are installed in CSs, we introduce the decision binary variables x_l and y_k for the l-th BS and the k-th RIS, respectively. Taking x_l as an example, $x_l = 1$ if the l-th BS is installed and $x_l = 0$ otherwise. These decision variables allow us to determine the optimal placement for deploying the BSs and RISs in the CSs. As a result, we have,

$$\begin{cases} \alpha_{l,t} \le x_l,\ \beta_{l,k,t} \le x_l,\ \gamma_{l,k,t} \le x_l, & \forall l, \forall k, \forall t \in \mathcal{T}, \\ \beta_{l,k,t} \le y_k,\ \gamma_{l,k,t} \le y_k, & \forall l, \forall k, \forall t \in \mathcal{T}. \end{cases} \tag{16}$$

Meanwhile, each RIS assists up to one BS at a time,[5] i.e.,

$$\sum_l \max_t \beta_{l,k,t} \le 1,\ \sum_l \max_t \gamma_{l,k,t} \le 1, \quad \forall k. \tag{17}$$

In this paper, we further consider that the deployment cost of the infrastructures (BSs and RISs) does not exceed the total cost ζ^{tot}, i.e.,

$$\sum_l x_l \zeta^B + \sum_k y_k \zeta^R \le \zeta^{\text{tot}}, \tag{18}$$

with ζ^B and ζ^R indicating the cost of installing one BS and one RIS, respectively.

3) CONSTRAINTS AMONG THE BS, RIS, AND UE

As shown in Figure 2, to guarantee that the RIS can receive signals from the BS and reflect it to the desired UE, both the BS and UE must be in front of the RIS, namely, the projection of the vector pointing from the k-th RIS to the l-th BS, $\boldsymbol{b}_l - \boldsymbol{r}_k$, and the vector pointing from the k-th RIS to the t-th UE, $\boldsymbol{u}_t - \boldsymbol{r}_k$, over a orientation vector of the k-th RIS, $\boldsymbol{n}_k$, requires to be positive, i.e.,

$$\begin{cases} \beta_{l,k,t} \boldsymbol{n}_k^T (\boldsymbol{u}_t - \boldsymbol{r}_k) \ge 0, & \forall l, \forall k, \forall t \in \mathcal{T}, \\ \beta_{l,k,t} \boldsymbol{n}_k^T (\boldsymbol{b}_l - \boldsymbol{r}_k) \ge 0, & \forall l, \forall k, \forall t \in \mathcal{T}, \\ \gamma_{l,k,t} \boldsymbol{n}_k^T (\boldsymbol{u}_t - \boldsymbol{r}_k) \ge 0, & \forall l, \forall k, \forall t \in \mathcal{T}, \\ \gamma_{l,k,t} \boldsymbol{n}_k^T (\boldsymbol{b}_l - \boldsymbol{r}_k) \ge 0, & \forall l, \forall k, \forall t \in \mathcal{T}. \end{cases} \tag{19}$$

B. PROBLEM FORMULATION

We aim to evaluate the performance of RIS-aided mmWave networks from two distinct perspectives, namely connectivity maximization (CM) and EMF exposure minimization (EM). In terms of CM optimization problem, our goal is to maximize the number of served UEs while satisfying the QoS of each UE and limited EMF exposure constraints. Furthermore, according to (14) and (15), we can derive the equivalently achievable data rate r_t of the t-th UE by substituting (20), as shown at the bottom of the next page, into (3). Hence, the CM optimization problem $\mathscr{P}1$ can be formulated as follows:

$$\begin{aligned} \mathscr{P}1\ (\text{CM}):\ & \max_{\substack{\boldsymbol{\alpha},\boldsymbol{\beta},\boldsymbol{\gamma},\boldsymbol{x},\boldsymbol{y},\\ \boldsymbol{w},\boldsymbol{\theta}}} \sum_{l,k,t} (\alpha_{l,t} + \beta_{l,k,t} + \gamma_{l,k,t}) \\ & \text{s.t. C1}: \sum_{k,t} (\alpha_{l,t} + \beta_{l,k,t} + \gamma_{l,k,t}) \left\| \boldsymbol{w}_{l,t} \right\|^2 \le P_{\max},\ \forall l, \\ & \quad \text{C2}: \sum_{l,k} (\alpha_{l,t} + \beta_{l,k,t} + \gamma_{l,k,t}) R_t^{\min} \le r_t,\ \forall t \in \mathcal{T}, \\ & \quad \text{C3}: E_{\max} \le E_{\lim}, \\ & \quad (14)\text{–}(19), \end{aligned}$$

where $\boldsymbol{\alpha} = \{\alpha_{l,t}\}$, $\boldsymbol{\beta} = \{\beta_{l,k,t}\}$, $\boldsymbol{\gamma} = \{\gamma_{l,k,t}\}$, $\boldsymbol{x} = \{x_l\}$, $\boldsymbol{y} = \{y_k\}$, $\boldsymbol{w} = \{\boldsymbol{w}_{l,t}\}$, and $\boldsymbol{\theta} = \{\boldsymbol{\theta}_k\}$. $P_{\max}$ is the maximum transmit power of the BS, and $R_t^{\min}$ denotes the minimum required data rate of the t-th UE. $E_{\lim}$ represents the limit for EMF exposure in ICNIRP for the frequency of 28 GHz [15]. C1 enforces that the BS power budget is satisfied by the precoder while C2 guarantees that each UE meets the minimum data rate requirement. C3 ensures that the EMF exposure in each grid does not exceed $E_{\lim}$. Furthermore, we are concerned with minimizing the global EMF exposure while ensuring the QoS of each UE and maintaining the connectivity. Hence, the EM optimization problem $\mathscr{P}2$ can be formulated as follows:

$$\begin{aligned} \mathscr{P}2\ (\text{EM}):\ & \min_{\substack{\boldsymbol{\alpha},\boldsymbol{\beta},\boldsymbol{\gamma},\boldsymbol{x},\boldsymbol{y},\\ \boldsymbol{w},\boldsymbol{\theta}}} E \\ & \text{s.t. C4}: \frac{\sum_{l,k,t} (\alpha_{l,t} + \beta_{l,k,t} + \gamma_{l,k,t})}{|\mathcal{T}|} \ge \text{CR}, \\ & \quad \text{C1, C2, and } (14)\text{–}(19), \end{aligned}$$

where $|\mathcal{T}|$ denotes the cardinality of $\mathcal{T}$, and $\text{CR} \in [0, 1]$ represents the coverage rate.

Due to the intricate interdependence between the BS, RIS and UE associations, as well as the presence of non-convex C2 where the transmit beamforming and phase shifts are coupled, problem $\mathscr{P}1$ and $\mathscr{P}2$ are NP-hard. For example, even given a specific association between the BS, RIS and UE, there are no optimal solutions. Typically, the problem is solved by relaxing as a convex semidefinite programming with high computational complexity or alternatively solving the separate optimizations until convergence to find sub-optimal solutions [9], [10], [22].

IV. RIS-AIDED NETWORK PLANNING

To address the difficulties of the CM and EM problems, we first transform the nonlinear constraints to the linear constraints, and then propose a power-efficient algorithm to solve these transformed problems effectively. For simplicity, if not specified, all the subscripts l, k, t in the remaining context are arbitrary.

[4] Similarly to other mmWave planning works [21], [32], in real-life scenarios, network operators usually determine the appropriate locations based on logistical, administrative and physical constraints, such as the geographic environment, the density of UEs, and etc.

[5] In practice, each BS can leverage on multiple RISs but each RIS is used and controlled by a single BS, which connects to the on-board RIS controller via a separate (wired or wireless) reliable control link.

A. TRANSFORMATION

To reduce the complexity of problem $\mathscr{P}1$ and $\mathscr{P}2$, we first transform the nonlinear constraints to the linear constraints.

1) LINEARIZE (17)

We define the binary variables $\mu_{l,k}$ and $\nu_{l,k}$ as

$$\mu_{l,k} := \max(\beta_{l,k,1}, \ldots, \beta_{l,k,t}, \ldots, \beta_{l,k,|\mathcal{T}|}), \tag{21}$$

$$\nu_{l,k} := \max(\gamma_{l,k,1}, \ldots, \gamma_{l,k,t}, \ldots, \gamma_{l,k,|\mathcal{T}|}). \tag{22}$$

Consequently, (17) can be rewritten as

$$\sum_{l} \mu_{l,k} \leq 1, \quad \text{and} \quad \sum_{l} \nu_{l,k} \leq 1. \tag{23}$$

By introducing the auxiliary binary variables $z_{l,k,t}$ and $\hat{z}_{l,k,t}$, (21) and (22) can be equivalently linearly substituted by

$$\begin{cases} \mu_{l,k} \geq \beta_{l,k,t}, \\ \beta_{l,k,t} \geq \mu_{l,k} - R_1(1 - z_{l,k,t}), \\ \sum\limits_{t} z_{l,k,t} \geq 1, \end{cases} \tag{24}$$

and

$$\begin{cases} \nu_{l,k} \geq \gamma_{l,k,t}, \\ \gamma_{l,k,t} \geq \nu_{l,k} - R_1(1 - \hat{z}_{l,k,t}), \\ \sum\limits_{t} \hat{z}_{l,k,t} \geq 1, \end{cases} \tag{25}$$

respectively, where R_1 is a positive real number and can take the value of 1 here. Eventually, (17) can be equivalently replaced by (23)–(25).

2) LINEARIZE C3

Since both $E_{\max}$ and $E_{\lim}$ are positive numbers, to eliminate the root formula effect of (13), we can rewrite C3 as

$$(E_{\max})^2 \leq (E_{\lim})^2, \tag{26}$$

where $(E_{\max})^2 = \max\{(E_i^{\text{tot}})^2\}$. Note that only when the l-th BS is installed, there will be the EMF exposure from the l-th BS for the i-th grid, i.e., based on (13), we have,

$$(E_i^{\text{tot}})^2 = \sum_{l=1}^{L} (x_l E_{l,i})^2 = \sum_{l=1}^{L} x_l (E_{l,i})^2, \tag{27}$$

where $x_l^2 = x_l$, as $x_l \in \{0, 1\}$. Similarly, by introducing a binary variable $\tilde{z}_i$, we have,

$$\begin{cases} (E_{\max})^2 \geq (E_i^{\text{tot}})^2, \\ (E_i^{\text{tot}})^2 \geq (E_{\max})^2 - R_2(1 - \tilde{z}_i), \\ \sum\limits_{i} \tilde{z}_i \geq 1, \end{cases} \tag{28}$$

where R_2 is a large positive real number. As a result, C3 can be equivalently replaced by (26) and (28).

3) LINEARIZE C2

To obtain the theoretical upper bound performance gains for the RIS-aided mmWave networks, we adopt a time-sharing process for the RIS, where each RIS is allowed to assist one BS-UE pair at a time. This implies an instantaneous reconfiguration of the reflecting elements when the RIS switches between different BS-UE pairs [21]. Accordingly, we can focus on optimizing the individual beamforming patterns of each RIS to enhance the coverage of mmWave communication systems. By leveraging the propagation and reflective properties of mmWave communication and RIS, (20) can be then approximated by the signal-to-noise ratio (SNR) [20], i.e.,

$$\eta_t = \Big| \sum_{l,k} \Big(\beta_{l,k,t} \boldsymbol{g}_{k,t}^H \boldsymbol{\Theta}_k \boldsymbol{G}_{l,k} + \alpha_{l,t} \boldsymbol{h}_{l,t}^H + \gamma_{l,k,t} \left(\boldsymbol{g}_{k,t}^H \boldsymbol{\Theta}_k \boldsymbol{G}_{l,k} + \boldsymbol{h}_{l,t}^H \right) \Big) \boldsymbol{w}_{l,t} \Big|^2 / \sigma_t^2. \tag{29}$$

To simplify the analysis, we consider the adoption of the maximum ratio transmission (MRT) precoding vector at the BS. In these conditions, we then derive the optimal beamforming vectors for each UE for different channels. Firstly, for only BS-UE channel, i.e., $\sum_{l,t} \alpha_{l,t} \geq 1$, $\sum_{l,k,t} \beta_{l,k,t} = \sum_{l,k,t} \gamma_{l,k,t} = 0$, we have,

$$\boldsymbol{w}_{l,t} = \frac{\sqrt{p_{l,t}^{\text{ue}}} \boldsymbol{h}_{l,t}}{\|\boldsymbol{h}_{l,t}\|}, \tag{30}$$

where $p_{l,t}^{\text{ue}}$ is the transmit power from the l-th BS to the t-th UE via BS-UE channel. Consequently, C2 can be simplified as (see Appendix A for the derivation)

$$\alpha_{l,t} \left(2^{R_t^{\min}/B} - 1 \right) \sigma_t^2 \leq \|\boldsymbol{h}_{l,t}\|^2 p_{l,t}^{\text{ue}}, \quad \forall l, \forall t \in \mathcal{T}. \tag{31}$$

Then, in terms of only BS-RIS-UE channel, i.e., $\sum_{l,k} \beta_{l,k,t} \geq 1$, $\sum_{l} \alpha_{l,t} = \sum_{l,k} \gamma_{l,k,t} = 0$, we have,

$$\boldsymbol{w}_{l,t} = \frac{\sqrt{p_{l,k,t}^{\text{ris}}} \left(\boldsymbol{g}_{k,t}^H \boldsymbol{\Theta}_k \boldsymbol{G}_{l,k} \right)^H}{\left\| \left(\boldsymbol{g}_{k,t}^H \boldsymbol{\Theta}_k \boldsymbol{G}_{l,k} \right)^H \right\|}, \tag{32}$$

where $p_{l,k,t}^{\text{ris}}$ is the transmit power from the l-th BS to the t-th UE via BS-RIS-UE channel. To obtain the optimal $\boldsymbol{\Theta}_k$, $\bar{\boldsymbol{\Theta}}_k$, we define $\bar{\boldsymbol{g}}_{k,t} := \boldsymbol{g}_{k,t}^* \circ \boldsymbol{a}_N \left(\psi_{l,k}^{(0)}, \hat{\psi}_{l,k}^{(0)} \right)$, in which $\circ$ denotes the Hadamard (elementwise) product. According

$$\eta_t = \frac{\left| \sum_{l,k} \left(\beta_{l,k,t} \boldsymbol{g}_{k,t}^H \boldsymbol{\Theta}_k \boldsymbol{G}_{l,k} + \alpha_{l,t} \boldsymbol{h}_{l,t}^H + \gamma_{l,k,t} \left(\boldsymbol{g}_{k,t}^H \boldsymbol{\Theta}_k \boldsymbol{G}_{l,k} + \boldsymbol{h}_{l,t}^H \right) \right) \boldsymbol{w}_{l,t} \right|^2}{\sum_{j \neq t} \left| \sum_{l,k} \left(\beta_{l,k,j} \boldsymbol{g}_{k,t}^H \boldsymbol{\Theta}_k \boldsymbol{G}_{l,k} + \alpha_{l,j} \boldsymbol{h}_{l,t}^H + \gamma_{l,k,j} \left(\boldsymbol{g}_{k,t}^H \boldsymbol{\Theta}_k \boldsymbol{G}_{l,k} + \boldsymbol{h}_{l,t}^H \right) \right) \boldsymbol{w}_{l,j} \right|^2 + \sigma_t^2}. \tag{20}$$

to [9], we can find the optimal value of $\boldsymbol{\theta}_k, \bar{\boldsymbol{\theta}}_k$, as follows:

$$\bar{\boldsymbol{\theta}}_k = \left[e^{-j\arg\left(\bar{g}_{k,t}^1\right)}, \ldots, e^{-j\arg\left(\bar{g}_{k,t}^N\right)} \right]^T, \tag{33}$$

where $\arg(x)$ denotes the argument of the complex number x, and $\bar{g}_{k,t}^n$ denotes the n-th entry of $\bar{\boldsymbol{g}}_{k,t}$. Thus, the optimal diagonal phase shift matrix is given as

$$\bar{\boldsymbol{\Theta}}_k = \operatorname{diag}\left(\bar{\boldsymbol{\theta}}_k\right). \tag{34}$$

By substituting (34) into (32), C2 can then be simplified as

$$\beta_{l,k,t}\left(2^{R_t^{\min}/B} - 1\right)\sigma_t^2 \leq \left\| \boldsymbol{g}_{k,t}^H \bar{\boldsymbol{\Theta}}_k \boldsymbol{G}_{l,k} \right\|^2 p_{l,k,t}^{\mathrm{ris}}, \quad \forall l, k, \forall t \in \mathcal{T}. \tag{35}$$

For the case of only COM-BS-RIS channel, i.e., $\sum_{l,k} \gamma_{l,k,t} \geq 1$, $\sum_l \alpha_{l,t} = \sum_{l,k} \beta_{l,k,t} = 0$, we have,

$$\boldsymbol{w}_{l,t} = \frac{\sqrt{p_{l,k,t}^{\mathrm{com}}}\left(\boldsymbol{g}_{k,t}^H \boldsymbol{\Theta}_k \boldsymbol{G}_{l,k} + \boldsymbol{h}_{l,t}^H\right)^H}{\left\| \left(\boldsymbol{g}_{k,t}^H \boldsymbol{\Theta}_k \boldsymbol{G}_{l,k} + \boldsymbol{h}_{l,t}^H\right)^H \right\|}, \tag{36}$$

where $p_{l,k,t}^{\mathrm{com}}$ is the transmit power from the l-th BS to the t-th UE via COM-BS-RIS channel. Similarly, we can obtain the optimal diagonal phase shift matrix [9], $\hat{\boldsymbol{\Theta}}_k$, as

$$\hat{\boldsymbol{\Theta}}_k = e^{j\tau_k} \operatorname{diag}\left(\bar{\boldsymbol{\theta}}_k\right), \tag{37}$$

where $\tau_k = -\arg\left(\boldsymbol{a}_M^T\left(\omega_{l,k}^{(0)}, \hat{\omega}_{l,k}^{(0)}\right)\boldsymbol{h}_{l,t}\right)$. By substituting (37) into (36), accordingly, C2 can be simplified as

$$\gamma_{l,k,t}\left(2^{R_t^{\min}/B} - 1\right)\sigma_t^2 \leq \left\| \left(\boldsymbol{g}_{k,t}^H \hat{\boldsymbol{\Theta}}_k \boldsymbol{G}_{l,k} + \boldsymbol{h}_{l,t}^H\right) \right\|^2 p_{l,k,t}^{\mathrm{com}}, \quad \forall l, k, \forall t \in \mathcal{T}. \tag{38}$$

Finally, C2 can be replaced by three independent constraints of (31), (35) and (38).

4) LINEARIZE C1

By introducing the transmit power variables, C1 can be readily linearized to

$$\sum_{k,t} \alpha_{l,t} p_{l,t}^{\mathrm{ue}} + \beta_{l,k,t} p_{l,k,t}^{\mathrm{ris}} + \gamma_{l,k,t} p_{l,k,t}^{\mathrm{com}} \leq P_{\max}, \quad \forall l. \tag{39}$$

B. RIS-AIDED POWER-EFFICIENT ALGORITHM

In this subsection, we will develop the RIS-aided power-efficient network planning (RISP) algorithm by applying the equivalent linear transformations of the main constraints mentioned earlier.

The core idea underlying the RISP algorithm is to allocate transmit power to each UE in a straightforward manner, ensuring the fulfillment of their minimum QoS requirements, thereby optimizing power efficiency. For instance, in the context of the CM problem, since our objective is to maximize the connectivity, it is not necessary for the BS to allocate more than the minimum required transmit power to the UE. Moreover, although minimizing EMF exposure is the main goal of the EM problem, due to the of existence of C4, the EM problem can be formulated to some extent as the CM problem (see Appendix B). Consequently, we can adopt a straightforward approach to determine the optimal transmit power for both the CM and EM problems, with a focus on achieving power efficiency.

Proposition 1: The optimal transmit power for BS-UE channel, BS-RIS-UE channel, and COM-BS-RIS channel is

$$\begin{cases} P_{l,t}^{\mathrm{ue}} = \dfrac{\left(2^{R_t^{\min}/B} - 1\right)\sigma_t^2}{\left\|\boldsymbol{h}_{l,t}\right\|^2}, & \text{(40a)} \\ P_{l,k,t}^{\mathrm{ris}} = \dfrac{\left(2^{R_t^{\min}/B} - 1\right)\sigma_t^2}{\left\|\boldsymbol{g}_{k,t}^H \bar{\boldsymbol{\Theta}}_k \boldsymbol{G}_{l,k}\right\|^2}, \text{ and,} & \text{(40b)} \\ P_{l,k,t}^{\mathrm{com}} = \dfrac{\left(2^{R_t^{\min}/B} - 1\right)\sigma_t^2}{\left\|\left(\boldsymbol{g}_{k,t}^H \hat{\boldsymbol{\Theta}}_k \boldsymbol{G}_{l,k} + \boldsymbol{h}_{l,t}^H\right)\right\|^2}, & \text{(40c)} \end{cases}$$

respectively.

Proof: Without loss of generality, we consider the scenario where only the BS-UE channel exists, i.e., $\sum_{l,t} \alpha_{l,t} \geq 1$, $\sum_{l,k,t} \beta_{l,k,t} = \sum_{l,k,t} \gamma_{l,k,t} = 0$. Based on (31), when a UE is accessed, the minimum required transmit power is

$$P_{l,t}^{\mathrm{ue}} = \frac{\left(2^{R_t^{\min}/B} - 1\right)\sigma_t^2}{\left\|\boldsymbol{h}_{l,t}\right\|^2}. \tag{41}$$

For any given l-th BS, by substituting (41) into (39), we assume that

$$\sum_t \alpha_{l,t} P_{l,t}^{\mathrm{ue}} = P_{\max}. \tag{42}$$

On this basis, if there is $p_{l,t}^{\mathrm{ue}} > P_{l,t}^{\mathrm{ue}}$ in (31), it implies that the inequality $\sum_t \alpha_{l,t} p_{l,t}^{\mathrm{ue}} > P_{\max}$ holds, which is contrary to the constraint (39). The proposition is proven. □

Taking into account the optimal power allocation scheme in **Proposition 1**, (39) can be rewritten as

$$\sum_{k,t} \alpha_{l,t} P_{l,t}^{\mathrm{ue}} + \beta_{l,k,t} P_{l,k,t}^{\mathrm{ris}} + \gamma_{l,k,t} P_{l,k,t}^{\mathrm{com}} \leq P_{\max}, \quad \forall l. \tag{43}$$

Undoubtedly, (43) is arguable a crucial constraint, as it not only eliminates the transmit power variables but also guarantees that the total transmit power remains is within a specified limit. Since all constraints are characterized as linear forms, we can now reformulate the original CM problem $\mathscr{P}1$ as

$\mathscr{P}3$ (Transformed CM) :

$$\max_{\substack{\boldsymbol{\alpha},\boldsymbol{\beta},\boldsymbol{\gamma},\boldsymbol{x},\boldsymbol{y},\\ \boldsymbol{\mu},\boldsymbol{\nu},\boldsymbol{z}}} \sum_{l,k,t} (\alpha_{l,t} + \beta_{l,k,t} + \gamma_{l,k,t})$$

s.t. (14)–(16), (18)–(19), (23)–(25), (26), (28), (31), (35), (38), and (43),

Algorithm 1 RIS-Aided Power-Efficient Network Planning

Input: $R_t^{\min}$, $P_{\max}$, $E_{\lim}$, B, L, K, $|\mathcal{T}|$, ϖ
Output: $\sum_{l,k,t}(\alpha_{l,t}+\beta_{l,k,t}+\gamma_{l,k,t}), E$

```
// determine
for t ∈ T do
    for k = 1, ..., K do
        calculate the optimal diagonal matrices, Θ̄_k and Θ̂_k, by (34) and (37), respectively
        for l = 1, ..., L do
            calculate the optimal transmit power, P^ue_{l,t}, P^ris_{l,k,t}, and P^com_{l,k,t} by (40a)
            α_{l,t} ← 0 if P^ue_{l,t} > P_max
            β_{l,k,t} ← 0 if P^ris_{l,k,t} > P_max
            γ_{l,k,t} ← 0 if P^com_{l,k,t} > P_max
        end for
    end for
end for
// solve
solve the transformed CM problem, P3
solve the transformed EM problem, P4
```

where $\boldsymbol{\mu} = \{\mu_{l,k}\}$, $\boldsymbol{\nu} = \{\nu_{l,k}\}$, and $\boldsymbol{z} = \{z_{l,k,t}, \hat{z}_{l,k,t}, \tilde{z}_i\}$. Similarly, the EM problem $\mathscr{P}2$ can be transformed to

$$\mathscr{P}4\ (\text{Transformed EM}):\quad \min_{\substack{\boldsymbol{\alpha},\boldsymbol{\beta},\boldsymbol{\gamma},\boldsymbol{x},\boldsymbol{y},\\ \boldsymbol{\mu},\boldsymbol{\nu},\boldsymbol{z}}} \quad E$$

$$\text{s.t. (14)–(16), (18)–(19), (23)–(25), (31), (35), (38), (43), and C4.}$$

Following the aforementioned, we can now proceed to devise the RISP algorithm. The RISP algorithm consists of two key stages: *determine* and *solve*. Specifically, in the *determine* stage, for the given t-th UE, l-th BS and k-th RIS, we initially calculate the optimal diagonal matrices by (34) and (37), and substitute them into (40a) to obtain the optimal transmit power for each UE with respect to different channels. Subsequently, since the transmit power is not allowed to exceed the maximum power of the BS, we can readily determine the infeasible association between the UE, BS and RIS to reduce the complexity. In the *solve* stage, since the transformed CM and EM problem are integer linear programming (ILP) problems, we can efficiently solve it by Gurobi solver to obtain the optimal solution with the well-established methods such as the Branch-and-Bound (B&B). We present the RISP algorithm in **Algorithm 1**.

V. PERFORMANCE EVALUATION

In this section, we first describe the simulation environment configuration, and then provide numerical results to evaluate the performance of the proposed RISP algorithm.

TABLE 2. Simulation parameters.

Parameters	Values	Parameters	Values
B	200 MHz	M	16
f_c	28 GHz	N	$\{200, 400, 800\}$
$P_{\max}$	30 dBm	$\lvert\mathcal{T}\rvert$	30
σ_t^2	-90 dBm	$\mathcal{R}$	100 m × 100 m
L, K	10	ζ^B	1
$E_{\lim}$	61.4 V/m	ζ^R	0.5

A. SIMULATION ENVIRONMENT

1) PARAMETER CONFIGURATION

We consider a three-dimensional (3D) coordinate system where 10 BSs, each deployed with a ULA comprising 16 antennas, and 10 RISs, each equipped with a UPA consisting of {200, 400, 800} reflecting elements, serve the UEs in a set $\mathcal{T}$. We assume that the UEs are randomly distributed within a square region $\mathcal{R}$ of 100 m × 100 m, while the BSs and RISs are deployed in CSs.

The maximum transmit power of the BS and the power of noise at the t-th UE are set as $P_{\max} = 30$ dBm and $\sigma_t^2 = -90$ dBm, respectively. The carrier frequency for downlink is set as $f_c = 28$ GHz, and the bandwidth B is set to 200 MHz [33]. We consider 4 NLOS paths, and the inter-element spacing d is set to $0.5\lambda_c$ [5], [6]. According to the exposure reference levels outlined by ICNIRP [15], the incident power density should not exceed 10 W/m^2, which is approximately equivalently converted to 61.4 $(\sqrt{10 \times 377})$ V/m. Therefore, $E_{\lim}$ is set to 61.4 V/m. For simplicity and analysis, the cost associated with the installation of a single BS and a single RIS is normalized as $\zeta^B = 1$ and $\zeta^R = 0.5$, respectively. The main simulation parameters are summarized in Table 2, unless otherwise specified.

2) CHANNEL CONFIGURATION

According to [5], the mmWave distance-dependent path loss model can be estimated as

$$PL^{\hat{X}}(D) = \varrho_a + \varrho_b 10\log_{10}(D) + \xi, \quad \xi \sim \mathcal{N}\left(0, \sigma_\xi^2\right), \quad (44)$$

where $\hat{X} \in \{\text{LOS, NLOS}\}$, D denotes the distance in meters between the transmitter and receiver, and ξ represents shadowing fading with σ_ξ^2 being the lognormal shadowing variance. The value of ϱ_a, ϱ_b and σ_ξ can be set to $\varrho_a = 61.4$, $\varrho_b = 2$ and $\sigma_\xi = 5.8$ dB for $\hat{X} = \text{LOS}$, respectively, or $\varrho_a = 72$, $\varrho_b = 2.92$ and $\sigma_\xi = 8.7$ dB for $\hat{X} = \text{NLOS}$, respectively. Based on (4), the BS-UE channel can be further rewritten as

$$\boldsymbol{h}_{l,t} = \sqrt{\frac{M}{U_{l,t}}}\left(\sqrt{\frac{\epsilon}{1+\epsilon}}\kappa_{l,t}^{(0)}\boldsymbol{a}_M\left(\phi_{l,t}^{(0)}, \hat{\phi}_{l,t}^{(0)}\right) + \sqrt{\frac{1}{1+\epsilon}}\sum_{\ell=1}^{U_{l,t}}\kappa_{l,t}^{(\ell)}\boldsymbol{a}_M\left(\phi_{l,t}^{(\ell)}, \hat{\phi}_{l,t}^{(\ell)}\right)\right), \quad (45)$$

where ϵ denotes the Rician factor and is set to be 10, and the complex gain $\kappa_{l,t}^{(\ell)}$ can be generated according to a complex

Gaussian distribution [5]

$$\begin{cases} \kappa_{l,t}^{(0)} \sim \mathcal{CN}\left(0,\ 10^{-0.1PL^{\hat{X}}\left(D_{l,t}^{\mathrm{BU}}\right)}\right), & \hat{X} = \mathrm{LOS}, \\ \kappa_{l,t}^{(\ell)} \sim \mathcal{CN}\left(0,\ 10^{-0.1PL^{\hat{X}}\left(D_{l,t}^{\mathrm{BU}}\right)}\right), & \hat{X} = \mathrm{NLOS}, \end{cases} \tag{46}$$

where $D_{l,t}^{\mathrm{BU}}$ denotes the distance in meters between the l-th BS and the t-th UE. On the other hand, as previously mentioned in (9) and (10), we only consider the LOS path of the RIS-aided channels. Consequently, the complex gain $\iota_{k,t}^{(0)}$ in (9) and $\rho_{l,k}^{(0)}$ in (10) can be generated by

$$\begin{cases} \iota_{k,t}^{(0)} \sim \mathcal{CN}\left(0,\ 10^{-0.1PL^{\hat{X}}\left(D_{k,t}^{\mathrm{RU}}\right)}\right), & \hat{X} = \mathrm{LOS}, \\ \rho_{l,k}^{(0)} \sim \mathcal{CN}\left(0,\ 10^{-0.1PL^{\hat{X}}\left(D_{l,k}^{\mathrm{BR}}\right)}\right), & \hat{X} = \mathrm{LOS}, \end{cases} \tag{47}$$

respectively, where $D_{k,t}^{\mathrm{RU}}$ and $D_{l,k}^{\mathrm{BR}}$ represent the distance in meters between the k-th RIS and the t-th UE, and between the l-th BS and the k-th RIS, respectively.

B. NUMERICAL RESULTS

To evaluate the performance of RIS-aided mmWave networks addressed by the RISP algorithm, we consider the scenario without RISs as a benchmark. We assess the performance of the system from two distinct perspectives, i.e., connectivity maximization (CM) and EMF exposure minimization (EM). All simulation results are averaged over 1000 independent channel realizations.

1) RESULTS FOR THE CM PROBLEM

We first evaluate the CM problem, which aims to maximize the number of served UEs under the EMF exposure constraints. Additionally, in order to characterize the impact of the EMF exposure on the system performance, we also consider a scenario without the EMF exposure constraints for comparison.

In Figure 3, we study the impact of the maximum transmit power of the BS ($P_{\max}$) on the downlink connectivity to investigate how much gain we can obtain with the RISP algorithm. The minimum required data rate for each UE is set as $R_t^{\min} = 1.0$ Gbps and the total cost is set as $\zeta^{\mathrm{tot}} = 10$. Figure 3 shows that the system incorporating the RIS outperforms the system without the RIS. Specifically, there is an approximately maximum improvement of 19.5% and 15.2% on served UEs for the system with and without EMF exposure constraints, respectively. This highlights the significant enhancement in the connectivity achieved through the RIS, regardless of the presence or absence of EMF exposure constraints. Moreover, from Figure 3, we can observe that when considering the EMF exposure constraints, the number of served UEs initially increases, reaching a peak at approximately $P_{\max} = 24$ dBm, and then decreases as $P_{\max}$ increases from 24 dBm to 30 dBm. This trend can be attributed to the fact that an initial increase in transmit power

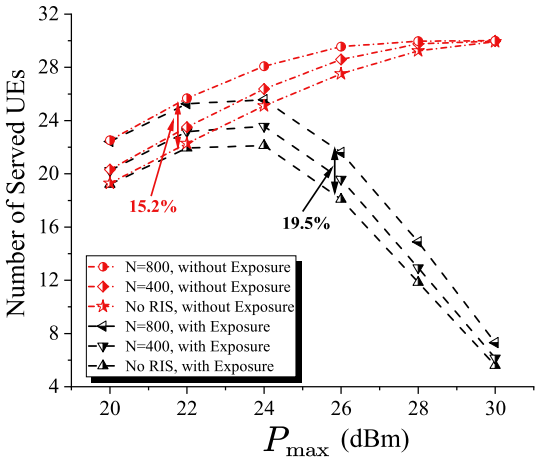

FIGURE 3. Number of served UEs versus the maximum transmit power of the BS, $P_{\max}$, with $R_t^{\min} = 1.0$ Gbps and $\zeta^{\mathrm{tot}} = 10$.

enhances the connectivity without reaching the exposure limit. However, further increasing the transmit power results in a corresponding rise in EMF exposure, due to the presence of $E_{\lim}$, thereby leading to a reduction in the connectivity. On the other hand, without the EMF exposure constraints, due to the total number of devices being set to 30, the number of served UEs increases with $P_{\max}$ until 30 is reached with different convergence rates. Moreover, as expected, equipping more reflecting elements at the RIS, leading to less path loss and a higher SINR, provides the improved system performance.

Figure 4 illustrates the impact of the minimum required data rate of the UE ($R_t^{\min}$) on the downlink connectivity. Based on the results in Figure 3, we set $P_{\max}$ and ζ^{tot} to be 24 dBm and 10, respectively, for optimal performance. We can learn from Figure 4 that due to the fixed $P_{\max}$, the number of served UEs decreases with the increase of $R_t^{\min}$ from 0.6 Gbps to 1.6 Gbps for both the system with and without EMF exposure constraints. Moreover, employing more reflecting elements at the RIS leads to improved performance. In particular, with the RIS, the system can achieve a maximum performance improvement of 17.1% and 16.1% on connectivity for the system with and without EMF exposure constraints, respectively.

Figure 5 provides the results of the system throughput ($\sum_{l,k,t}(\alpha_{l,t}+\beta_{l,k,t}+\gamma_{l,k,t})R_t^{\min}$) plotted against the total cost (ζ^{tot}) where $P_{\max}$ and $R_t^{\min}$ are set to be 24 dBm and 1.0 Gbps, respectively. Figure 5 shows that the system throughput exhibits a positive correlation with the total cost and reaches a stable state after around $\zeta^{\mathrm{tot}} = 10$, when the EMF exposure constraints are present. This finding is arguably significant as it suggests that further increments in cost do not lead to performance enhancement due to EMF exposure constraints, which is valuable for network operators as it helps them find an optimal trade-off between system performance and cost. For instance, in this case, the optimal value of the total cost is 10. Moreover, as expected, the presence of the

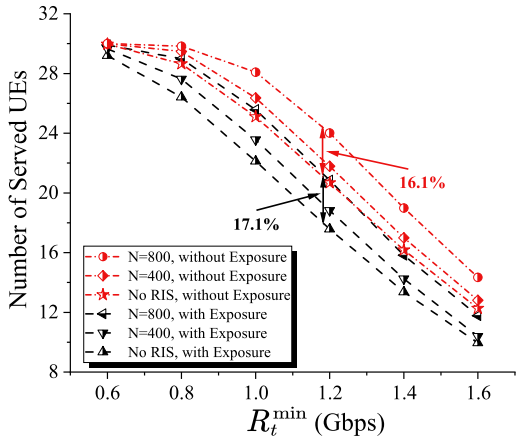

FIGURE 4. Number of served UEs versus the minimum required data rate of the UE, $R_t^{\min}$, with $P_{\max} = 24$ dBm and $\zeta^{\text{tot}} = 10$.

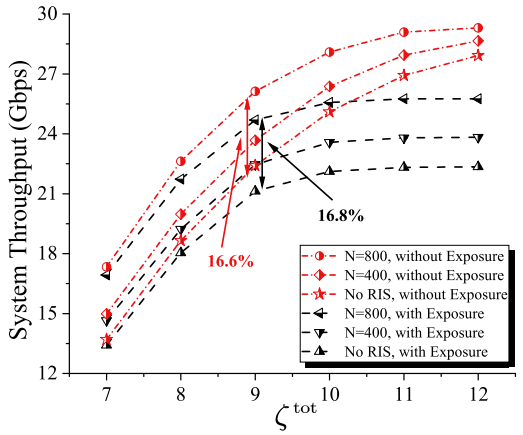

FIGURE 5. System throughput versus the total cost, ζ^{tot}, with $P_{\max} = 24$ dBm and $R_t^{\min} = 1.0$ Gbps.

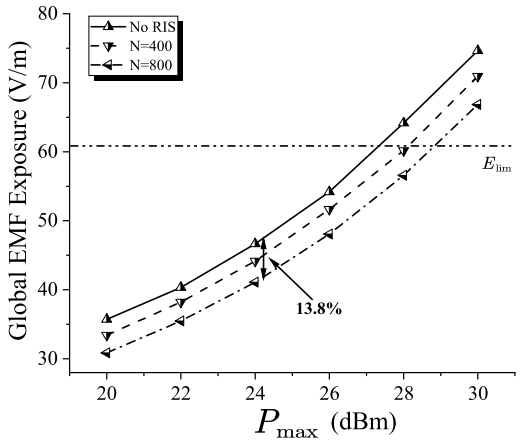

FIGURE 6. Global EMF exposure versus the maximum transmit power of the BS, $P_{\max}$, with $R_t^{\min} = 0.6$ Gbps, CR = 90%, $\varpi = 0.5$ and $\zeta^{\text{tot}} = 15$.

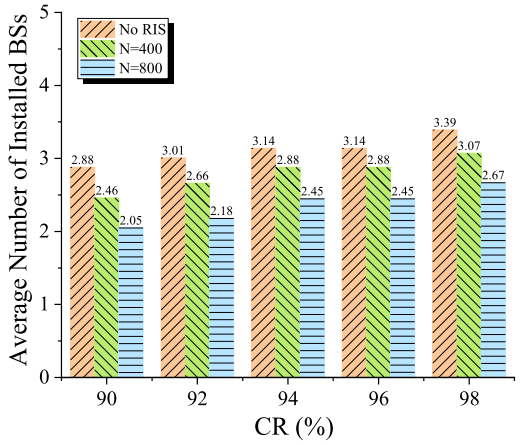

FIGURE 7. Average number of installed BSs versus the coverage rate (CR), with $K = 10$, $P_{\max} = 28$ dBm, $R_t^{\min} = 0.6$ Gbps, $\varpi = 0.5$ and $\zeta^{\text{tot}} = 15$.

RIS contributes to improved system performance, with up to approximately 17% enhancement.

2) RESULTS FOR THE EM PROBLEM

Different from the CM problem mentioned above, the EM problem focuses on minimizing the global EMF exposure while satisfying the coverage rate (CR) requirement.

In Figure 6, we plot the global EMF exposure versus the maximum transmit power of the BS ($P_{\max}$), where $R_t^{\min} = 0.6$ Gbps, CR = 90%, $\varpi = 0.5$ and $\zeta^{\text{tot}} = 15$. From Figure 6, it is evident that the global EMF exposure increases as $P_{\max}$ increases, which indicates that higher transmit power results in elevated EMF exposure levels in the system. Additionally, it can be observed that the system without the RIS is the first to exceed E_{lim} at approximately $P_{\max} = 27$ dBm. Interestingly, as the number of reflecting elements at the RIS increases, the global EMF exposure decreases, and this reduction can be as much as 13.8%. This is due to the fact that with more reflecting elements, the RIS can effectively manipulate the signal propagation and improve the channel quality, allowing the UE to achieve the required QoS with lower transmit power. As a result, the global EMF exposure is reduced.

Figure 7 shows the average number of installed BSs versus the CR, where we fix the number of installed RISs, i.e., $K = 10$, and $P_{\max} = 28$ dBm, $R_t^{\min} = 0.6$ Gbps, $\varpi = 0.5$ and $\zeta^{\text{tot}} = 15$. The average number of installed BSs increases gradually with the CR. However, it is noteworthy that the presence of RISs can effectively reduce the average number of installed BSs. This is because, for a given CR, with the assistance of RISs, the system can achieve better connectivity and access a larger number of UEs, thereby reducing the reliance on additional BS installations. In particular, with RISs, there is a reduction of up to about 28.8% in the number of BSs installations.

In Figure 8, we present the empirical cumulative distribution function (CDF) of the global EMF exposure, where $P_{\max} = 28$ dBm, $R_t^{\min} = 0.6$ Gbps, $\varpi = 0.5$, CR = 90% and $\zeta^{\text{tot}} = 15$. The global EMF exposure of the system with the RIS is consistently lower than that of the system without the RIS at the same probability. This result aligns with the

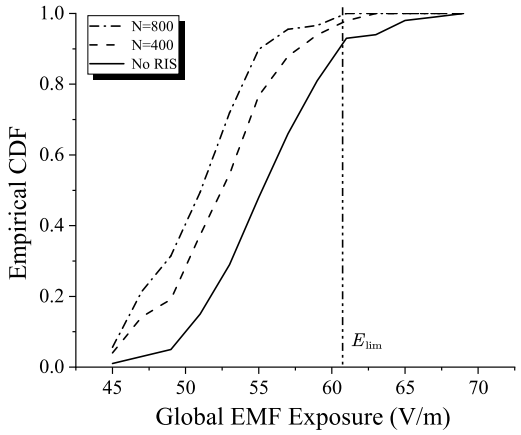

FIGURE 8. Empirical cumulative distribution function (CDF) of the global EMF exposure with $P_{\max} = 28$ dBm, $R_t^{\min} = 0.6$ Gbps, $\varpi = 0.5$, CR = 90% and $\zeta^{\text{tot}} = 15$.

findings in Figure 6, indicating that the presence of RIS can effectively reduce the global EMF exposure in the system. Additionally, as the number of reflecting elements in the RIS increases, the performance of the system improves, with a higher probability of achieving lower global EMF exposure levels.

VI. CONCLUSION

In this paper, we investigate a RIS-aided multi-user downlink MISO mmWave network planning framework. The objective is to maximize connectivity and minimize EMF exposure by leveraging the capabilities of the RIS to assist in communication between the BS and UE. We formulate the network planning problem as a MINLP problem, considering the joint optimization of infrastructure placement and link associations. To tackle these problems, we first transform them into a MILP problem and then develop a power-efficient algorithm for effective solutions. Simulation results demonstrate the superior performance of the RIS-aided mmWave networks, outperforming conventional benchmarks that do not employ the RIS in terms of both connectivity and EMF exposure, achieving up to an approximately 20% improvement in connectivity and 14% reduction in EMF exposure. In future work, we aim to extend the proposed model to large-scale network planning. In addition, MIMO systems with more practical scenarios such as imperfect CSI and beam alignment will also be the next direction of our research. Given the complexity of the optimization problem, we believe that machine learning will be a promising approach to tackle this challenge.

APPENDIX A

Without loss of generality, considering that the BS communicates with the UE only via BS-UE channel, based on (30), C2 can be rewritten as

$$\sum_l \alpha_{l,t} R_t^{\min} \le B \log_2 \left(1 + \frac{\sum_l \alpha_{l,t} \left\|\boldsymbol{h}_{l,t}\right\|^2 p_{l,t}^{\text{ue}}}{\sigma_t^2}\right), \ \forall t \in \mathcal{T}. \tag{48}$$

Due to (14), there is at most one item not being zero on the left side of formula (48). (48) can be further expressed as

$$\sum_l \alpha_{l,t} R_t^{\min} \le B \log_2 \left(1 + \frac{\alpha_{1,t} \left\|\boldsymbol{h}_{1,t}\right\|^2 p_{1,t}^{\text{ue}} + , \ldots, + \alpha_{L,t} \left\|\boldsymbol{h}_{L,t}\right\|^2 p_{L,t}^{\text{ue}}}{\sigma_t^2}\right). \tag{49}$$

From (49), we can further obtain

$$\left(2^{\frac{(\sum_l \alpha_{l,t}) R_t^{\min}}{B}} - 1\right) \sigma_t^2 \le \alpha_{1,t} \left\|\boldsymbol{h}_{1,t}\right\|^2 p_{1,t}^{\text{ue}} + , \ldots, + \alpha_{L,t} \left\|\boldsymbol{h}_{L,t}\right\|^2 p_{L,t}^{\text{ue}}. \tag{50}$$

According to the affine transformation, we can finally get

$$\alpha_{l,t} \left(2^{R_t^{\min}/B} - 1\right) \sigma_t^2 \le \left\|\boldsymbol{h}_{l,t}\right\|^2 p_{l,t}^{\text{ue}}, \quad \forall l, \forall t \in \mathcal{T}. \tag{51}$$

APPENDIX B

The problem $\mathscr{P}2$ can be simply described as

$$\begin{aligned} \mathscr{P}2': \ & \min \ E \\ & \text{s.t.} \ \sum_{l,k,t} (\alpha_{l,t} + \beta_{l,k,t} + \gamma_{l,k,t}) \ge |\mathcal{T}| \text{CR}, \\ & \quad \text{other constraints}, \end{aligned}$$

where E is a function of x_l for $l = 1, \ldots, L$, i.e., $E = f(x_l)$, which means for any given values $x_1, \ldots, x_L$, E is uniquely determined. Assuming that the values of $x_l, \ldots, x_L$ are given, then problem $\mathscr{P}2'$ can be transformed to

$$\begin{aligned} \mathscr{P}2'': \ & \max \sum_{l,k,t} (\alpha_{l,t} + \beta_{l,k,t} + \gamma_{l,k,t}) \\ & \text{s.t. other constraints}. \end{aligned}$$

If the result of problem $\mathscr{P}2''$, $\sum_{l,k,t}(\alpha_{l,t} + \beta_{l,k,t} + \gamma_{l,k,t})$, satisfies the constraint $\sum_{l,k,t}(\alpha_{l,t} + \beta_{l,k,t} + \gamma_{l,k,t}) \ge |\mathcal{T}|\text{CR}$, then problem $\mathscr{P}2'$ is considered partially solved. Otherwise, the value of $x_l, \ldots, x_L$ is iteratively chosen until the constraint is met. Eventually, the E with the minimum value among all the results of $\mathscr{P}2'$ is selected as the solution of problem $\mathscr{P}2$.

REFERENCES

[1] Q. Wu, S. Zhang, B. Zheng, C. You, and R. Zhang, "Intelligent reflecting surface-aided wireless communications: A tutorial," *IEEE Trans. Commun.*, vol. 69, no. 5, pp. 3313–3351, May 2021.
[2] *Cisco Annual Internet Report (2018–2023) White Paper*, Cisco, San Jose, CA, USA, Aug. 2020, pp. 1–35.
[3] T. Bai and R. W. Heath, "Coverage and rate analysis for millimeter-wave cellular networks," *IEEE Trans. Wireless Commun.*, vol. 14, no. 2, pp. 1100–1114, Feb. 2015.
[4] S. Rangan, T. S. Rappaport, and E. Erkip, "Millimeter-wave cellular wireless networks: Potentials and challenges," *Proc. IEEE*, vol. 102, no. 3, pp. 366–385, Mar. 2014.
[5] M. R. Akdeniz, Y. Liu, M. K. Samimi, S. Sun, S. Rangan, T. S. Rappaport, and E. Erkip, "Millimeter wave channel modeling and cellular capacity evaluation," *IEEE J. Sel. Areas Commun.*, vol. 32, no. 6, pp. 1164–1179, Jun. 2014.
[6] O. E. Ayach, S. Rajagopal, S. Abu-Surra, Z. Pi, and R. W. Heath, "Spatially sparse precoding in millimeter wave MIMO systems," *IEEE Trans. Wireless Commun.*, vol. 13, no. 3, pp. 1499–1513, Mar. 2014.

[7] T. S. Rappaport, S. Sun, R. Mayzus, H. Zhao, Y. Azar, K. Wang, G. N. Wong, J. K. Schulz, M. Samimi, and F. Gutierrez, "Millimeter wave mobile communications for 5G cellular: It will work!" *IEEE Access*, vol. 1, pp. 335–349, 2013.

[8] E. Basar, M. Di Renzo, J. De Rosny, M. Debbah, M.-S. Alouini, and R. Zhang, "Wireless communications through reconfigurable intelligent surfaces," *IEEE Access*, vol. 7, pp. 116753–116773, 2019.

[9] P. Wang, J. Fang, X. Yuan, Z. Chen, and H. Li, "Intelligent reflecting surface-assisted millimeter wave communications: Joint active and passive precoding design," *IEEE Trans. Veh. Technol.*, vol. 69, no. 12, pp. 14960–14973, Dec. 2020.

[10] Q. Wu and R. Zhang, "Intelligent reflecting surface enhanced wireless network via joint active and passive beamforming," *IEEE Trans. Wireless Commun.*, vol. 18, no. 11, pp. 5394–5409, Nov. 2019.

[11] Z. Li, H. Hu, J. Zhang, and J. Zhang, "Coverage analysis of multiple transmissive RIS-aided outdoor-to-indoor mmWave networks," *IEEE Trans. Broadcast.*, vol. 68, no. 4, pp. 935–942, Dec. 2022.

[12] L. Chiaraviglio, A. Elzanaty, and M.-S. Alouini, "Health risks associated with 5G exposure: A view from the communications engineering perspective," *IEEE Open J. Commun. Soc.*, vol. 2, pp. 2131–2179, 2021.

[13] G. Castellanos, S. De Gheselle, L. Martens, N. Kuster, W. Joseph, M. Deruyck, and S. Kuehn, "Multi-objective optimisation of human exposure for various 5G network topologies in Switzerland," *Comput. Netw.*, vol. 216, Oct. 2022, Art. no. 109255.

[14] A. Elzanaty, L. Chiaraviglio, and M.-S. Alouini, "5G and EMF exposure: Misinformation, open questions, and potential solutions," *Frontiers Commun. Netw.*, vol. 2, Apr. 2021, Art. no. 635716.

[15] International Commission on Non-Ionizing Radiation Protection, "Guidelines for limiting exposure to electromagnetic fields (100 kHz to 300 GHz)," *Health Phys.*, vol. 118, no. 5, pp. 483–524, May 2020.

[16] S. Q. Wali, A. Sali, J. K. Allami, and A. F. Osman, "RF-EMF exposure measurement for 5G over mm-wave base station with MIMO antenna," *IEEE Access*, vol. 10, pp. 9048–9058, 2022.

[17] A. Zappone and M. D. Renzo, "Energy efficiency optimization of reconfigurable intelligent surfaces with electromagnetic field exposure constraints," *IEEE Signal Process. Lett.*, vol. 29, pp. 1447–1451, 2022.

[18] H. Ibraiwish, A. Elzanaty, Y. H. Al-Badarneh, and M.-S. Alouini, "EMF-aware cellular networks in RIS-assisted environments," *IEEE Commun. Lett.*, vol. 26, no. 1, pp. 123–127, Jan. 2022.

[19] A. Subhash, A. Kammoun, A. Elzanaty, S. Kalyani, Y. H. Al-Badarneh, and M.-S. Alouini, "Optimal phase shift design for fair allocation in RIS aided uplink network using statistical CSI," *IEEE J. Sel. Areas Commun.*, vol. 41, no. 8, pp. 2461–2475, Aug. 2023.

[20] A. Albanese, G. Encinas-Lago, V. Sciancalepore, X. Costa-Pérez, D.-T. Phan-Huy, and S. Ros, "RIS-aware indoor network planning: The Rennes railway station case," in *Proc. IEEE Int. Conf. Commun. (ICC)*, Seoul, South Korea, May 2022, pp. 2028–2034.

[21] E. Moro, I. Filippini, A. Capone, and D. De Donno, "Planning mm-wave access networks with reconfigurable intelligent surfaces," in *Proc. IEEE 32nd Annu. Int. Symp. Pers., Indoor Mobile Radio Commun. (PIMRC)*, Helsinki, Finland, Sep. 2021, pp. 1401–1407.

[22] Y. Cao, T. Lv, and W. Ni, "Intelligent reflecting surface aided multi-user mmWave communications for coverage enhancement," in *Proc. IEEE 31st Annu. Int. Symp. Pers., Indoor Mobile Radio Commun.*, London, U.K., Aug. 2020, pp. 1–6.

[23] M. Nemati, J. Park, and J. Choi, "RIS-assisted coverage enhancement in millimeter-wave cellular networks," *IEEE Access*, vol. 8, pp. 188171–188185, 2020.

[24] P. Mursia, V. Sciancalepore, A. Garcia-Saavedra, L. Cottatellucci, X. C. Pérez, and D. Gesbert, "RISMA: Reconfigurable intelligent surfaces enabling beamforming for IoT massive access," *IEEE J. Sel. Areas Commun.*, vol. 39, no. 4, pp. 1072–1085, Apr. 2021.

[25] *Study on New Radio (NR) Access Technology*, document TR 38.912, Version 0.0.2, 3GPP, Sep. 2016.

[26] G. Zhou, C. Pan, H. Ren, P. Popovski, and A. L. Swindlehurst, "Channel estimation for RIS-aided multiuser millimeter-wave systems," *IEEE Trans. Signal Process.*, vol. 70, pp. 1478–1492, 2022.

[27] Y. Liu, S. Zhang, F. Gao, J. Tang, and O. A. Dobre, "Cascaded channel estimation for RIS assisted mmWave MIMO transmissions," *IEEE Wireless Commun. Lett.*, vol. 10, no. 9, pp. 2065–2069, Sep. 2021.

[28] J. He, H. Wymeersch, and M. Juntti, "Channel estimation for RIS-aided mmWave MIMO systems via atomic norm minimization," *IEEE Trans. Wireless Commun.*, vol. 20, no. 9, pp. 5786–5797, Sep. 2021.

[29] S. Noh, J. Lee, G. Lee, K. Seo, Y. Sung, and H. Yu, "Channel estimation techniques for RIS-assisted communication: Millimeter-wave and sub-THz systems," *IEEE Veh. Technol. Mag.*, vol. 17, no. 2, pp. 64–73, Jun. 2022.

[30] P. Wang, J. Fang, W. Zhang, Z. Chen, H. Li, and W. Zhang, "Beam training and alignment for RIS-assisted millimeter-wave systems: State of the art and beyond," *IEEE Wireless Commun.*, vol. 29, no. 6, pp. 64–71, Dec. 2022.

[31] M. Deruyck, E. Tanghe, D. Plets, L. Martens, and W. Joseph, "Optimizing LTE wireless access networks towards power consumption and electromagnetic exposure of human beings," *Comput. Netw.*, vol. 94, pp. 29–40, Jan. 2016.

[32] F. Devoti and I. Filippini, "Planning mm-wave access networks under obstacle blockages: A reliability-aware approach," *IEEE/ACM Trans. Netw.*, vol. 28, no. 5, pp. 2203–2214, Oct. 2020.

[33] T. Jiang, J. Zhang, M. Shafi, L. Tian, and P. Tang, "The comparative study of S-V model between 3.5 and 28 GHz in indoor and outdoor scenarios," *IEEE Trans. Veh. Technol.*, vol. 69, no. 3, pp. 2351–2364, Mar. 2020.

BO YIN received the B.Eng. degree in information engineering and the M.Eng. degree in information and communication engineering from the South China University of Technology, Guangzhou, China, in 2019 and 2022, respectively. He is currently pursuing the Ph.D. degree in electronics and ICT engineering with the Department of Information Technology, Ghent University, Belgium. His research interests include network planning, machine learning, and wireless communications.

WOUT JOSEPH (Senior Member, IEEE) was born in Ostend, Belgium, in October 1977. He received the M.Sc. degree in electrical engineering from Ghent University, Belgium, in July 2000, and the Ph.D. degree, in March 2005. His Ph.D. work dealt with measuring and modeling of electromagnetic fields around base stations for mobile communications related to the health effects of the exposure to electromagnetic radiation. From 2007 to 2012, he was a Postdoctoral Fellow of the Research Foundation—Flanders (FWO-V). Since October 2009, he has been a professor in the domain of experimental characterization of wireless communication systems. He has been an IMEC PI, since 2017. His research interests include electromagnetic field exposure assessment, propagation for wireless communication systems, antennas, and calibration. He specializes in wireless performance analysis and quality of experience.

MARGOT DERUYCK (Member, IEEE) was born in Kortrijk, Belgium, in July 1985. She received the M.Sc. degree in computer science engineering and the Ph.D. degree from Ghent University, Ghent, Belgium, in 2009 and 2015, respectively. From September 2009 to January 2015, she was a Research Assistant with the Department of Information Technology, IMEC–Wireless, Acoustics, Environment and Expert Systems (WAVES), Ghent University. Her scientific work is focused on green wireless access networks with minimal power consumption and minimal exposure from human beings. This work led to the Ph.D. degree. Since January 2015, she has been a Postdoctoral Researcher with Ghent University, where she currently continues her work in the green wireless access networks. She is also a Postdoctoral Fellow of the Research Foundation Flanders (FWO-V).